Dissociative adsorption of methane on surface oxide structures of Pd-Pt alloys

Arezoo Dianat,[1,*] Nicola Seriani,[2] Lucio Colombi Ciacchi,[3,4]
Wolfgang Pompe,[1] Gianaurelio Cuniberti,[1] Manfred Bobeth[1]

[1] *Institute for Materials Science and Max Bergmann Center of Biomaterials , Dresden University of Technology, D-01062 Dresden, Germany*

[2] *Fakultät Physik, Universität Wien, Sensengasse 8, 1090 Wien, Austria*

[3] *Hybrid Materials Interfaces Group, Faculty of Production Engineering and Bremen Centre for Computational Materials Science, University of Bremen, D-28359 Bremen, Germany*

[4] *Fraunhofer Institute for Manufacturing Technology and Applied Material Research IFAM, D-28359 Bremen, Germany*

March 23, 2010

Abstract

The dissociative adsorption of methane on variously oxidized Pd, Pt and Pd-Pt surfaces is investigated using density-functional theory, as a step towards understanding the combustion of methane on these materials. For Pd-Pt alloys, models of surface oxide structures are built on the basis of known oxides on Pd and Pt. The methane adsorption energy presents large variations depending on the oxide structure and composition. Adsorption is endothermic on the bare Pd(111) metal surface as well as on stable thin layer oxide structures such as the $(\sqrt{5}\times\sqrt{5})$ surface oxide on Pd(100) and the PtO_2-like oxide on Pt(111). Instead, large adsorption energies are obtained for the (100) surface of bulk PdO, for metastable mixed $Pd_{1-x}Pt_xO_{4/3}$ oxide layers on Pt(100), and for Pd-Pt(111) surfaces covered with one oxygen monolayer. In the latter case, we find a net thermodynamic preference for a direct conversion of methane to methanol, which remains adsorbed on the oxidized metal substrates via weak hydrogen-bond interactions.

* To whom correspondence should be addressed: arezoo.dianat@nano.tu-dresden.de

1 Introduction

The catalytic oxidation of hydrocarbons in general, and of methane in particular, is considered as an effective method of power generation associated with low emissions of CO_2 and NO_x. Because of the high H/C ratio of methane, the heat of combustion per mole of generated CO_2 is higher than for other fuels, e.g. twice as much as for coal [1]. The interest towards the development and optimization of novel catalysts for the combustion of methane has thus considerably increased over the last years. Especially palladium-based catalysts have been extensively explored because of their high catalytic oxidation activity. Among those catalysts, the bimetallic system Pd-Pt has been the object of many investigations [2–11]. In several studies it was found that Pd-Pt catalysts exhibit higher methane conversion efficiency [3–6, 8–12] and better long-term stability [3, 7, 11] than pure Pd.

The performance of Pd-Pt catalysts strongly depends on the chemical state of the metal surface at the conditions suitable for oxidation, which in many cases lead to the formation of superficial oxide phases. For pure Pd and Pt catalysts, there is agreement that oxide formation has a positive effect on their methane oxidation activity [13, 14], although the active oxide phases have not been unequivocally determined yet. On the one hand, some authors have proposed that bulk PdO is less active than either a thin oxide layer [15] or a layer of adsorbed oxygen on Pd [16, 17]. On the other hand, the formation of bulk oxide has been suggested to explain the observed increase in catalytic activity [18, 19]. Recently, Gabasch et al. [20] reported that bulk PdO seeds grown on a surface, otherwise covered by a Pd_5O_4 surface oxide, are the active phase for methane oxidation on a Pd(111) single crystal surface. The catalytic behavior of pure Pt metal is quite different. According to investigations in Refs. [18, 19, 21, 22], its catalytic activity reaches a maximum at a submonolayer coverage of adsorbed oxygen, and further oxidation with formation of PtO_2 leads to activity loss. Still, it is unclear whether a similar behavior can be expected also for other Pt oxide phases that could develop in an oxidizing atmosphere. Platinum bulk oxide phases comprise α-PtO_2, β-PtO_2, Pt_3O_4 and PtO [23–25]. Correspondingly, a large variety of surface oxides can be expected [26–28]. Previous calculations have suggested that Pt_3O_4

might be an active phase for the catalytic oxidation of carbon compounds [27]. Similarly, in the case of palladium, besides PdO also other bulk oxide phases could form, as e.g. PdO_2 [29]. Different surface oxides have been observed on Pd(111) [30–32], Pd(100) [33] and on stepped surfaces [34].

Compared with the large amount of data available for pure Pd and Pt, little is known about the oxidation behavior of the bimetal Pd-Pt and its relation to the higher catalytic activity displayed by these alloys. Persson et al. [10] suggested that Pd-Pt catalysts on alumina consist of a PdO-rich phase coexisting with a palladium-rich Pd-Pt alloy. Studying the composition dependence of the catalytic activity of Pd-Pt, Lapisardi et al. [11] found the highest activity for catalysts with very high Pd content $Pd_{0.93}Pt_{0.07}/Al_2O_3$.

In a previous study [35], we have investigated by means of density-functional theory (DFT) the thermodynamic stability of mixed bulk oxides $Pd_{1-x}Pt_xO_y$ isostructural to known bulk oxide phases of pure Pd and Pt. According to these calculations, the mixed oxide phase $Pd_{1-x}Pt_xO_2$ with crystal structure analogous to α-PtO_2 is stable only at rather low temperature (< 500 K for atmospheric oxygen pressure). With increasing temperature, a phase mixture of PdO with first PtO_2 and later Pt_3O_4 becomes stable. At higher temperature, the oxides decompose directly to metallic Pd-Pt, except for Pd-rich systems, where PdO and metallic Pt coexist within a small temperature window.

In the present DFT study, in a first step we analyze the stability of oxidized Pd-Pt surfaces as a basis for investigating their interaction with methane. Because of the lack of relevant experimental information, known surface oxide structures of pure Pd and pure Pt are used as guidelines to construct Pd-Pt surface oxide models. In a second step, we compute the driving forces for the dissociative adsorption of CH_4 on various oxidized Pd-Pt surfaces, which is commonly believed to be the rate-determining reaction in the catalytic combustion of methane.

The paper is outlined as follows. Computational details of the DFT analysis are briefly described in Sect. 2. In Sect. 3, we report on the calculated oxygen binding energies of various Pd-Pt oxide structures. The calculated methane adsorption energies on these oxide structures are then presented in Sect. 4. Finally, our results are discussed and interpreted

in relation to experimental findings in Sect. 5.

2 Computational details

Our DFT calculations are performed by means of the Vienna ab initio simulation package (VASP) [36–38], using the PBE generalized gradient approximation (GGA) for the exchange-correlation functional [39] and the PAW method [40,41]. The wave functions are expanded in plane waves up to a kinetic energy cut-off of 400 eV. The periodically repeated simulation cells include slabs of six substrate layers covered with either adsorbed oxygen or a thin oxide layer, and with adsorbed CH_3 and H. In all simulations, the vacuum gap between the slab surface models is larger than 15 Å. Unless stated otherwise, the size of the simulation cell corresponds to a (2×2) surface unit cell of the metal substrate. Integration in the first Brillouin zone is performed using Monkhorst-Pack grids [42] including 25 k-points in the irreducible wedge. In all calculations, the positions of all atoms are optimized until all force components become less than 0.01 eV/Å. Convergence of energy differences with respect to the used cut-off energies and k-point grids is ensured within a tolerance of 10 meV/atom. Further computational details can be found in Ref. [43].

3 Surface oxide structures on Pd-Pt

The oxidation of Pd and Pt surfaces proceeds from the chemisorption of oxygen atoms through the formation of surface oxides to the development of bulk oxide. In the case of palladium, the structure of surface oxide phases has been the subject of many experimental [44–47] as well as theoretical [30, 33, 34, 45, 48–50] investigations. Phase diagrams of surface oxide structures in dependence on the chemical potential of oxygen have been thoroughly characterized for several surface orientations [30,33]. On Pd(111), chemisorbed oxygen at low coverage is arranged with a p(2×2) periodicity. At higher coverage, several surface oxide phases form and coexist, as observed in STM investigations accompanied by theoretical modelling [30, 44, 48]. On the contrary, on Pd(100) only one surface oxide has

been found [33, 45], consisting of two unit cells of PdO(101) over a $(\sqrt{5} \times \sqrt{5})$ Pd(100) cell. Investigations of oxide formation on platinum revealed the following. On Pt(111), the formation of a bulk-like, strongly distorted α-PtO_2 surface oxide was observed at an oxygen partial pressure of 0.5 atm and temperatures from 520-910 K [51, 52]. α-PtO_2 was predicted to be the stable low temperature phase also by DFT calculations [27, 35]. On Pt(100), DFT calculations suggest the formation of an α-PtO_2-like surface oxide at low temperature [27, 28] and the existence of a stability region for a Pt_3O_4-like oxide layer at higher temperature.

3.1 On-surface and sub-surface adsorbed oxygen

To characterize the binding strength of oxygen atoms adsorbed at metal surfaces, we calculate an average oxygen binding energy E_b per O atom according to the formula

$$E_b = \frac{1}{N_O}\left[E_{O@S} - E_S - \frac{N_O}{2}E_{O_2}\right] , \quad (1)$$

where $E_{O@S}$ is the total energy of the oxygen-metal system, E_S the energy of the bare metal substrate, E_{O_2} the energy of a free oxygen molecule, and N_O the number of O atoms. The oxygen atoms in formula (1) include oxygen located on the surface as well as in sub-surface positions. The calculated oxygen binding energies on (111) surfaces are listed in Table 1 for different oxygen coverages up to 1 monolayer (ML). The values in the last column are obtained for a stack of atomic layers with Pd in the surface layer, Pt in the sub-surface layer, and Pd in the remaining layers. In a previous DFT study [35], we have calculated oxygen adsorption energies on mixed Pd-Pt surface and sub-surface layers. For the considered Pd-Pt compositions and configurations, the oxygen adsorption energies have been found to vary between -1.26 eV and -0.94 eV. In the case of stacks of pure Pd and Pt layers, we have obtained an adsorption energy of -0.99 eV on Pt/Pd/Pd(111) and -1.26 eV on Pd/Pt/Pd(111). The latter value presents the strongest oxygen binding that we have found on all considered stacks of mixed metal layers. This strong binding has been attributed to charge transfer from Pd to Pt which causes a strong binding between the more electropositive Pd atoms and electronegative O atoms.

The most stable oxygen adsorption sites on the (111) surface of Pd and Pt are the fcc hollow sites [53,54]. According to the energy values in Table 1, the oxygen binding energies on pure Pt(111) are significantly smaller than on pure Pd(111) for all considered coverages. The strongest oxygen binding is found for the Pd/Pt/Pd(111) layer stack.

Further calculations are performed for the case of fixed sub-surface oxygen coverage of 0.25 ML, and increasing on-surface coverage up to 0.75 ML, thus giving a maximum total coverage of 1 ML. Between the first and second metal layer there are three high-symmetry positions: an octahedral site underneath the fcc on-surface hollow site, a tetrahedral site (tetra I) below the hcp on-surface hollow site, and a second tetrahedral site (tetra II) directly below a surface metal atom [53]. For simultaneous on-surface and sub-surface adsorption, the fcc hollow site on the surface and the tetra I sub-surface position are found to be the most stable oxygen positions for all considered oxygen coverages. The corresponding average oxygen binding energies are given in Table 1 (referred to as on+sub). They reveal that, in addition to on-surface adsorption, oxygen incorporation underneath the surface layer becomes favorable for a total oxygen coverage $\theta_{\mathrm{tot}} \geq 0.75$ ML on Pd(111), and for $\theta_{\mathrm{tot}} = 1$ ML on Pt(111). This result is in agreement with other DFT calculations for Pd(111) [53]. For solely on-surface adsorption, the binding of oxygen is slightly stronger on Pd/Pt/Pd(111) than on Pd(111), whereas with sub-surface oxygen the average binding energy is larger for pure Pd(111) due to the unfavorable binding of oxygen to the Pt sub-surface layer in the case of Pd/Pt/Pd(111).

3.2 Thin oxide layers

With increasing oxygen coverage, surface oxide phases start forming on Pd and Pt surfaces. To our knowledge, there is no experimental information concerning the structure of such phases on the Pd-Pt bimetal. For this reason, model structures of possible Pd-Pt surface oxides are constructed here on the basis of the known oxide structures of pure Pd and Pt. In particular, we consider the experimentally observed PdO(101)-like [33, 45] and the theoretically predicted Pt_3O_4-like [27] oxide layers on the (100) surface, as well as the α-

PtO_2-like [27, 51] layer on the (111) surface. According to our previous calculations [35], these layers are characterized by small lattice misfits between oxide and metallic substrate, namely 2% for PdO(101)/Pd(100), 3.5% for α-PtO_2(0001)/Pt(111), and less than 1% for Pt_3O_4(100)/Pt(100). The corresponding oxide structures obtained after DFT geometry optimization are shown in Fig. 1.

In the case of PdO(101)/Pd(100), the Pd atoms of the oxide are located above the surface hollow sites of the substrate. The oxygen amount in the oxide layer corresponds to a coverage of 0.8 ML, referred to the surface metal atoms. In the case of α-PtO_2(0001)/Pt(111), the Pt atoms of the oxide are located above top sites, fcc hollow sites, as well as hcp hollow sites of the substrate, and the oxygen coverage is 1.5 ML. The epitaxial Pt_3O_4(100)/Pt(100) oxide layer corresponds to an oxygen coverage of 1 ML. In this case, the oxide layer includes two metal layers (cf. Figs. 1(e) and (f)).

In the case of mixed Pd-Pt systems, we consider special Pd-Pt configurations in the oxide layers and in the metal surface layers which are generated by the following replacements. For example, starting from a pure Pd system in the case of Fig. 1a, we first replace Pd atom 1 in the oxide layer by Pt. With increasing Pt concentration in this layer Pd atoms 2, 3 and 4 are replaced by Pt. The Pt concentration in the metal surface layer is increased in the same manner starting with Pd atom 5. For the other two layer systems (Figs. 1c and 1e), the Pt atoms are replaced by Pd in analogous manner.

In order to characterize the stability of oxide structures with different Pd-Pt configurations and variable oxygen coverage, an average oxygen binding energy can be defined as

$$E_b = \frac{1}{N_O}\left[E_{Layer@S} - E_S - N_{Pd}^{Layer}E_{Pd}^{bulk} - N_{Pt}^{Layer}E_{Pt}^{bulk} - \frac{N_O}{2}E_{O_2}\right] , \qquad (2)$$

where $E_{Layer@S}$ is the total energy of the substrate together with the oxide layer, E_S the energy of the substrate alone, E_{Pd}^{bulk} and E_{Pt}^{bulk} the energies of Pd and Pt atoms in their bulk phases, and N_O, N_{Pd}^{Layer} and N_{Pt}^{Layer} the numbers of oxygen, Pd, and Pt atoms in the oxide layer. The binding energy (2) corresponds to the energy gained by deposition of molecular oxygen and formation of an oxide with metal atoms from ideal bulk metal reservoirs. With

this definition we neglect the difference of chemical potentials of the metal atoms in the pure metal bulk and in a Pd-Pt alloy. Since the free energy of mixing of Pd-Pt is of the order of few tens of meV per metal atom, while the oxygen binding energies are of the order of one eV, this approximation will not significantly influence our conclusions.

To study the effect of the Pd-Pt composition on the oxygen binding energy, we vary the Pd/Pt ratio both in the oxide layer and in the outermost substrate-layer. All other substrate layers are composed of Pd in the case of the PdO(101) layer on Pd(100), and of Pt for the other two cases. The calculated oxygen binding energies for the three oxide layers are shown in Fig. 2 as a function of the Pt concentration of the outermost substrate layer. The different curves presented correspond to different compositions of the oxide layer. Every curve point represents one special Pd-Pt configuration as noted above. Test calculations for another configuration at fixed composition for $Pd_{0.5}Pt_{0.5}O$ on $Pd_{0.4}Pt_{0.6}$/Pd(100) and for α-$Pd_{0.33}Pt_{0.67}O_2$ on $Pd_{0.75}Pt_{0.25}$/Pt(111) yield only small differences in the average oxygen binding energy of 0.012 eV and 0.006 eV, respectively.

For the PdO(101) layer structure (Fig. 2(a)), the maximum variation of the oxygen binding energy with the substrate-layer composition is less than 0.05 eV. Similarly, the binding energy varies less than 0.1 eV for the α-PtO_2 structure (Fig. 2(b), note the different energy scale). Replacement of Pd atoms of the PdO-like layer with Pt is energetically unfavorable. Namely, the O binding energy changes from -1.15 to -0.90 eV passing from a pure PdO to a pure PtO layer. The same holds for replacing Pt atoms of the α-PtO_2 layer with Pd. An analogous result has previously been found for mixed *bulk* oxides of Pd-Pt [35]. For the case of the Pt_3O_4-like oxide layer (Fig. 2(c)), the changes in the binding energy with the substrate-layer composition are also small (less than 0.12 eV). For this oxide layer it is very unfavorable to replace Pt atoms with Pd. Indeed, a Bader analysis [55, 56] reveals that the oxygen atoms in Pd_3O_4/Pt(100) gain 0.67 e from metal atoms, while the corresponding value for Pt_3O_4/Pt(100) is 0.73 e, reflecting the stronger oxygen binding in the latter case. For the other two oxide structures considered, the charge transfer from metal atoms to oxygen does not change significantly with variation of the Pd-Pt composition in the oxide layer, consistently with the calculated small differences in

the oxygen binding energy.

4 Dissociative adsorption of methane

The first important step in the catalytic oxidation of methane is its adsorption on the catalyst surface and dissociation into adsorbed methyl and hydrogen. To get a first insight into the catalytic activity of Pd-Pt catalysts for methane oxidation, we compute the thermodynamic driving force for this adsorption reaction on various oxide structures, in particular on the superficial oxides of Pd-Pt considered in the previous section. The adsorption energy for the dissociative adsorption of CH_4 to CH_3 and H is defined as

$$E_a = E_{CH_3\&H@S} - E_S - E_{CH_4} \ , \tag{3}$$

where $E_{CH_3\&H@S}$ is the total energy of methyl and hydrogen adsorbed on the substrate, E_S the energy of the substrate, and E_{CH_4} the energy of methane in the gas phase. We do not perform zero point energy corrections of the calculated adsorption energies since we think that these corrections lead to comparatively small shifts of energy values (see e.g. Ref. [57]), which is of minor importance for comparing adsorption energies on different systems as main goal of this study.

4.1 CH_4 adsorption on clean metal surfaces

We first report on our calculations concerning methane adsorption on pure metallic (111) and (100) surfaces. In agreement with other DFT calculations [58, 59], we find that on the (111) surface the most stable adsorption site for CH_3 is on top of metal atoms and for H on fcc hollow sites. This applies to pure Pd(111) and Pt(111) as well as to the Pd/Pt/Pd(111) layer stack with Pd in the surface and Pt in the sub-surface atomic layer. The calculated adsorption energies, shown in Table 2, are -0.08 eV for the Pt(111) surface and 0.19 eV for the Pd(111) surface. The positive value for Pd(111) corresponds to an endothermic reaction. This is in agreement with previous DFT calculations for methane adsorption on Pd(111) within the generalized gradient approximation (GGA) (E_a = 0.27 eV), whereas

an exothermic reaction was found by using the local density approximation (LDA) (E_a = -0.62 eV) [59]. For comparison, at the LDA level we obtain adsorption energies of -0.43 eV, -0.66 eV, and -0.45 eV on Pd(111), Pt(111), and Pd/Pt/Pd(111), respectively. Thus, for all considered systems, the LDA values are shifted roughly by -0.6 eV with respect to the GGA values.

In the case of all (100) surfaces, CH_3 on top of metal atoms and H on bridge sites are the most stable adsorption configurations. On Pd(100) and Pd/Pt/Pd(100), dissociative adsorption of methane is found to be endothermic, in agreement with DFT calculations in [60]. Only on Pt(100), methane adsorption is exothermic with an adsorption energy of -0.31 eV.

4.2 CH_4 adsorption on surfaces with adsorbed oxygen

After analyzing methane adsorption on clean metal surfaces, we investigate here the adsorption on metal surfaces covered with 1 ML oxygen. A first set of calculations is performed starting with 1 ML of oxygen adsorbed solely *on* the (111) surface. As initial condition for the DFT calculations, the following positions of adsorbed CH_3 and H are chosen: H always on top of oxygen atom, and (i) CH_3 on top of metal atom, (ii) CH_3 on top of oxygen atom, and (iii) CH_3 on hcp hollow site. For these three cases, the calculated adsorption energies after structural relaxation are listed in Table 2. The corresponding optimized atomic structures are shown in Figs. 3 and 4 for the Pd(111) and Pt(111) surfaces. The structures obtained for the Pd/Pt/Pd(111) layer stack are qualitatively the same as for Pd(111). The largest adsorption energies are obtained starting with CH_3 on top of a metal atom and H on top of an oxygen atom. In particular, the adsorption energy on Pd/Pt/Pd(111) is slightly higher than on Pd(111). In the latter two cases, structural optimization leads to a remarkable reconstruction of the adsorbate layer (Fig. 3(a)). Both the CH_3 group and the H atom move away from their initial adsorption sites and bind to the same O atom, thus forming an adsorbed methanol molecule. Notably, if CH_3 and H are initially placed over other adsorption sites on Pd(111), CH_3 and H also detach from the metal atoms, but bind

separately to different O atoms of the surface, resulting in adsorbed OH and CH_3O groups and no methanol formation. The same is found in the case of the Pt(111) surface where CH_3 and H remain bound to separate sites. In this case, the Pt atoms to which CH_3 is bound are lifted off the surface layer by 2.2 to 2.5 Å, depending on the initial configuration (cf. Fig. 4).

Analogous calculations of methane adsorption energies have been performed for surfaces covered with 0.75 ML oxygen on the surface and 0.25 ML in sub-surface positions. Again, three different initial positions of adsorbed CH_3 and H have been chosen: H always on top of oxygen, and (i) CH_3 on top of metal atom, (ii) CH_3 on top of oxygen atom, and (iii) CH_3 on fcc hollow site (oxygen vacancy). The largest adsorption energy results for CH_3 and H initially on top of oxygen for all considered surfaces (denoted by CH_3-fcc & H-fcc in Table 2). The energy values in Table 2 indicate that methane adsorption on surfaces with sub-surface oxygen is about 1 eV weaker than for the case of oxygen adsorbed solely *on* the surface. In the presence of sub-surface oxygen, methanol does not form spontaneously starting from the initial geometries above, H and CH_3 remaining separately bound to different oxygen atoms.

While in the simulations so far the formation of methanol takes place only on Pd(111) and Pd/Pt/Pd(111) with oxygen on-surface coverage, we now calculate the adsorption energy after methanol formation on all other surfaces, irrespective of the initial geometry choosen. To this end, a novel set of DFT structural relaxations is performed starting with methanol adsorbed on all surfaces, including those with subsurface oxygen, using the atomic configuration obtained for Pd(111). In all cases, the adsorption energies are higher than for separately adsorbed CH_3 and H, as reported in Table 2. As visible in Fig. 3(a), the methanol molecule remains loosely adsorbed to the surface, mainly via a hydrogen-bond between the OH group of methanol and a surface O atom. The methanol adsorption energies amount to -0.11 eV on Pd(111) and Pd/Pt/Pd(111), and -0.08 eV on Pt(111) for 1 ML on-surface oxygen coverage, reflecting weak molecule-surface interactions.

4.3 CH_4 adsorption on superficial oxide layers

With increasing oxygen supply, the oxidation of the metallic catalyst is expected to proceed with formation of thin oxide layers. Correspondingly, we further investigate methane adsorption on the thin oxide layer structures described in Sect. 3.2. The most favorable adsorption sites of methyl and hydrogen are determined via relaxation of different structures with the following initial positions of the adsorbates: both CH_3 and H on top of oxygen or metal atoms, CH_3 on top of oxygen and H on top of metal atom, and vice versa. The optimized atomic structures on the PdO(101)/Pd(100), α-PtO_2(0001)/Pt(111), and Pt_3O_4(100)/Pt(100) layers are shown in Fig. 5. The Pd-Pt composition is varied both in the oxide layer and the outermost layer of the metal substrate (cf. Fig. 6). For all compositions, the stable atomic configurations of adsorbed CH_3 and H have been found to be qualitatively equal. However, the values of the adsorption energy, presented in Fig. 6, show comparatively large variations. Every curve point in Fig. 6 represents a special Pd-Pt configuration in the oxide and metal surface layer as described above. Test calculations of another Pd-Pt configuration for a PdO(101)- and PtO_2-like oxide layer at fixed composition (see Sect. 3.2) yield only small differences in the methane adsorption energy of less than 0.05 eV.

For the PdO(101)-like oxide layers, the most stable adsorption sites for CH_3 are either on Pd, if only Pd atoms are present, or on Pt, if Pt replaces Pd atoms in the oxide (Fig. 5(a)). The corresponding adsorption energy values (Fig. 6(a)) indicate that the methane decomposition reaction on this oxide structure is endothermic for all Pd-Pt compositions considered. As a general trend, for a given composition of the oxide layer, the reaction is the more endothermic the more Pd atoms are present in the outermost layer of the metal substrate, except for pure PtO(101) where the adsorption energy is independent of the substrate composition. For a given substrate composition, increasing the Pd/Pt ratio in the oxide from 0 to 1 results in a rather complex behavior of the adsorption energy values, whereby pure PtO(101) layer is the least reactive structure in all cases.

In the case of the α-PtO_2-like layer, where all metal atoms are fully coordinated by

oxygen, adsorption of both CH_3 and H occurs necessarily on the O atoms (Fig. 5(b)). The adsorption energy depends only weakly on the Pt concentration in the outermost substrate-layer, whereas a strong dependence on the oxide layer composition is observed (Fig. 6(b)). While the reaction is clearly endothermic for the pure PtO_2 oxide layer, it becomes exothermic for a Pd/Pt ratio in the oxide larger than about 0.5. Thus, the driving force for methane dissociation increases monotonously with the Pd content in the oxide.

In the case of the Pt_3O_4-like oxide layers, both CH_3 and H adsorb strongly on the undercoordinated exposed oxygen atoms (Fig. 5(c)), as found also previously for a pure Pt_3O_4 layer [27]. The adsorption energy of -1.74 eV obtained here is comparable to the value of -1.47 eV computed in Ref. [27] using norm-conserving pseudopotentials. Increasing the Pd concentration in the oxide layer leads to stronger and stronger adsorption, with little dependence on the composition of the outermost substrate-layer (Fig. 6(c)). In particular, the large adsorption energy of -2.5 eV, computed for the Pd_3O_4/Pt(100) oxide, is comparable to the driving force for methane dissociation and methanol formation computed for the case of an oxygen ML adsorbed on the Pd/Pt/Pd(111) surface (see Table 2).

4.4 CH_4 adsorption on bulk PdO-like oxides

After considering methane adsorption on thin oxide layers on Pd-Pt metal substrates, it is interesting to compute, for comparison, the methane adsorption energies on the corresponding bulk oxide surfaces. We note that for α-PtO_2 the adsorption on a single layer is already representative of the behavior of the bulk oxide, which consists of stacked PtO_2 layers weakly bound by van der Waals forces [27]. Furthermore, the surface of bulk Pt_3O_4 with lowest surface energy is nearly identical to the surface of the thin oxide layer considered above. In the following, we thus consider only surfaces of mixed Pd-Pt oxides with the structure of the well-known PdO bulk oxide phase. In particular, methane adsorption energies are calculated on the (100) and (101) surfaces, which present low surface energies [50].

As a model of a mixed oxide Pd-Pt-O, we analyze a slab of five PdO layers covered with a

mixed $Pd_{1-x}Pt_xO$ layer, in which Pd and Pt are arranged in a chess-like pattern for $x = 0.5$ (adsorption energies for the row-like Pd-Pt pattern differ less than 0.025 eV from the chess-like one). Our analysis shows that on the (100) surface CH_3 and H adsorb preferentially on top of oxygen atoms, in agreement with previous calculations [61] (Fig. 7(a)). On the (101) surface, H adsorbs on top of oxygen and CH_3 on top of metal atoms, preferentially on Pt in the case of a mixed Pd-Pt bulk oxide, as also found for the thin oxide layer in the previous section (Fig. 7(b)). The calculated adsorption energies on the different surfaces are listed in Table 3. With increasing Pt content in the oxide, a monotonously decreasing driving force for methane adsorption is found on PdO(100), whereas on Pd(101) the adsorption energy displays a non-trivial dependence on the Pt content, similarly as in the case of the thin Pd(101)-like oxide layer considered above. Unlike the case of thin PdO-like oxide layers, where methane adsorption is endothermic, for the PdO bulk phase, the adsorption reaction is exothermic. Regarding the dependence of the adsorption energy on the oxide composition, the largest value of -1.0 eV is obtained for the (100) surface of pure PdO (cf. Fig. 5(a)). This value is however considerably lower than the energy values calculated for the Pt_3O_4-like oxide layers on Pt(100) and for the oxygen adlayers on Pd(111) (cf. Fig. 6(c) and Table 2).

5 Discussion

The dissociative adsorption of methane on noble metal surfaces represents an essential reaction step of the catalytic combustion of methane, and is thought to limit the reaction kinetics. As a first effort towards a deeper understanding of this catalytic reaction, we have studied methane adsorption on various oxide structures of Pd, Pt and Pd-Pt alloy surfaces. The choice of the investigated systems is motivated by the facts that palladium oxide phases, in particular PdO, have been suggested to be catalytically more active than pure Pd [18, 19], and that mixed Pd-Pt catalysts have been found to possess higher conversion efficiency for methane combustion, especially on the long term. Our investigation includes chemisorbed O atoms, thin oxide layers and bulk PdO-like oxide surfaces, addressing both

their thermodynamic stability and their reactivity towards methane dissociation.

5.1 Formation of oxide layers on Pd-Pt surfaces

The thermodynamic stability of different oxidized Pd-Pt structures has been addressed by calculating average oxygen binding energies at 0 K. In general, superficial oxide layers are found to be more stable than oxygen adlayers(including sub-surface O atoms) at the corresponding oxygen coverages, as displayed in Table 2 and Fig. 2. The larger stability of oxygen adlayers on Pd compared to those on Pt can be understood simply from the lower electronegativity of palladium. Consistently with previous findings [43], the largest binding energy is found for a Pd/Pt/Pd(111) layer stack, due to the partial donation of electrons from the Pd surface layer to the Pt sub-surface layer, which increases the surface reactivity.

In the case of surface oxide layers, the Pd-Pt composition of the outermost layer of the metal substrate has only a minor influence on the oxygen binding strength. Changes of the binding strength due to varying the Pd/Pt ratio in the oxide can be explained on the basis of the stability of the corresponding bulk oxide phases, as thoroughly addressed in Refs. [27, 35]. Namely, mixed oxides with PdO structure are destabilized by replacing Pd atoms with Pt, while mixed oxides with α-PtO_2 or Pt_3O_4 structure are destabilized by replacing Pt atoms with Pd.

5.2 Dissociative adsorption of CH_4 on oxidized Pd-Pt surfaces

Concerning the dissociative adsorption of methane, our DFT calculations at the GGA level suggest, in agreement with existing literature [59], that Pd metal surfaces are not reactive, and Pt surfaces are only little reactive. Since CH_3 and H possess an electron-donor character, they are expected to bind better to electronegative elements. Indeed, binding to pure Pt (electronegativity 2.3 on the Pauling scale) is stronger than to pure Pd (electronegativity 2.2). However, if adsorbed oxygen (electronegativity 3.4) is present on the surface, either in the form of an oxygen adlayer or as surface oxide, then binding to

oxygen provides a strong driving force for methane dissociation.

Correspondingly, we have obtained the largest adsorption energies for 1 ML of oxygen adsorbed on the (111) metal surfaces, in particular on Pd(111) and on the Pd/Pt/Pd(111) layer stack, with an energy gain of about -2.4 eV (cf. Table 2). A peculiar effect observed on the latter two surfaces is the spontaneous formation of a methanol molecule which remains only loosely bound to the surface via hydrogen bonds and weak metal-oxygen interactions (Fig. 3(a)). We observe a net thermodynamic preference for methanol formation on all three surfaces considered, with the largest values being obtained on Pd(111). An analysis of the energy barriers associated with the $CH_4 \rightarrow CH_3OH$ conversion reaction exceeds the scope of the present investigation. However, the possibility of a direct methane to methanol conversion on the (111) surface of transition metals has been recently put forward in a theoretical DFT study [63]. It has to be noted, however, that the further combustion of methanol on Pd-Pt surfaces is expected to take place at the temperatures required to dissociate the C-H bonds of methane. Therefore, in general the selectivity towards methanol formation is found to decrease by increasing the overall conversion efficiency [64].

In the case of superficial oxide layers formed on Pd-Pt, we have found that methane adsorption is clearly endothermic both on the thin PdO(101)-like layer on (100) surfaces and on the thin α-PtO_2-like layer on (111) surfaces. Since the same was noted for oxidation of carbon monoxide [62], these phases may be considered as a kind of passivation layer on the metal substrate, whose formation may suddenly reduce the oxidation activity of the catalysts. This property, however, is not shared by the surfaces of bulk oxides, where both the (101) and the (100) surfaces are reactive towards methane dissociation (Table 3). This behavior can be understood by considering the charge transfer between the CH_3 molecule and the surface atoms. According to a Bader analysis, in the case of bulk PdO, the CH_3 molecule donates electrons to the surface and becomes positively charged (+0.44e), while in the case of the PdO-like oxide layer CH_3 gains electrons (-0.13e). This indicates a strongly reduced electronegativity of the metal atoms of the thin oxide layer due to the presence of the underlying metal substrate, compared with the surfaces of bulk oxides. As a consequence, binding of CH_3 to the surface of the bulk oxide is favorable, in contrast to

the oxide monolayer over the metal substrate. This finding is consistent with experimental observations that oxidation of Pd with formation of PdO is beneficial for methane oxidation [18, 19]. In comparison, bulk α-PtO_2 is inert with respect to methane dissociation in the absence of defects (see also Ref. [27]). This again is consistent with observations that formation of bulk oxide phases is beneficial for methane oxidation on Pd, but not on Pt [18, 19, 21]. Oxidation of Pt might be beneficial if the reaction conditions allow the formation of Pt_3O_4-like phases (see also the discussion in [24, 27, 28]). Namely, our DFT calculations predict adsorption energies of CH_3 and H on Pt_3O_4 and Pd_3O_4 which are higher than those on PdO surfaces and comparable with that on oxygen adlayers covering Pd(111). This is due to the availability of undercoordinated oxygen sites on the exposed Pt_3O_4(100) surface, to which electron acception from CH_3 and H is very favorable.

Concerning effects on methane adsorption resulting from Pd-Pt alloying, we note that in most of our calculations the composition of the metal substrate underneath the thin oxide layer does not show a pronounced effect on the methane adsorption energy. However, the effect of the composition of the oxide layer is evident and the reactivity decreases with increasing Pt content. An exception is the thin PdO(101)-like oxide layer on (100) surfaces, where the CH_3 group binds preferentially to the metal atom rather than to oxygen. In this case, the presence of Pt atoms does increase the reactivity since they are stronger electron acceptors, as mentioned above. However, at the same time the presence of Pt results in a decrease of the reactivity of the O atoms towards the adsorption of H. These two counteracting effects result in a non-trivial trend of the computed adsorption energies with increasing Pt content, both in the case of the thin layers (Fig. 6) and of bulk PdO(101) (Table 3). The actual adsorption energies in this case depend on the specific arrangements of Pt, Pd and O atoms close to the adsorption sites of CH_3 and H, both in the oxide layer and in the metal substrate. However, in none of the cases considered is the adsorption reaction exothermic, as discussed previously.

6 Conclusions

In conclusion, we have performed extensive calculations of the driving force for methane dissociation on clean and oxidized Pd-Pt surfaces. Both in the case of Pd and Pt, formation of stable thin layer oxide structures such as the PdO(101)-like layer on the (100) surface and the α-PtO_2-like layer on the (111) surface, leads to a reactivity loss towards the dissociative adsorption of methane. Methane adsorption is instead favored on metastable surface oxide structures such as a Pt_3O_4-like layer, whose reactivity increases with increasing Pd content. Furthermore, reactivity is recovered for exposed surfaces of *bulk* PdO, consistently with existing experimental results [6, 11].

In the case of oxygen adlayers we have found that the formation of a methanol molecule after methane dissociation is thermodynamically favored. This may suggest that selective conversion of methane to methanol rather than total oxidation can be achieved under pressure and temperature conditions that prevent the formation of surface oxides. However, the further combustion of the produced methanol over other sites of the Pd-Pt surface cannot be excluded, reducing the selectivity of the conversion reaction.

As a final remark, we would like to note that our investigation, being concerned with the thermodynamic driving force for the methane dissociation reaction, should be considered only as a preliminary indication about the reactivity of different surface structures. Based on the results presented here, more thorough calculations of the corresponding activation barriers, which can be directly related to the kinetic constants for adsorption, shall be the subject of forthcoming works.

Acknowledgments

Computational resources were provided by the Center for Information Services and High Performance Computing (ZIH) of the Technische Universität Dresden. This work was partially supported by the Deutsche Forschungsgemeinschaft under contract CI 144/1-2 and CU 44/9-2. LCC acknowledges support by the Deutsche Forschungsgemeinschaft within the Emmy Noether Programme. NS acknowledges support by the FWF.

References

[1] Y. Chin and D. E. Resasco, Catalysis, Vol. 14 (1999); Ed. J.J. Spivey, London, 1999.

[2] C. Micheaud, P. Matecot, M. Guerin, and J. Barbier, Appl. Catal. A: General 171 (1998) 229.

[3] K. Narui, H. Yata, K. Furuta, A. Nishida, Y. Kohtoku, and T. Matsuzaki, Appl. Catal. A: General 179 (1999) 165.

[4] A. Ersson, H. Kusar, R. Carroni, T. Griffin, and S. Jaras, Catal. Today 83 (2003) 265.

[5] Y. Deng and T. G. Nevell, Catal. Today 47 (1999) 279.

[6] H. Yammamoto and H. Uchida, Catal. Today 45 (1998) 147.

[7] Y. Ozawa, Y. Tochihara, A. Watanabe, M. Nagari, and S. Omi, Appl. Catal. A: General 259 (2004) 1.

[8] K. Persson, A. Ersson, A. M. Carrera, J. Jayasuriya, R. Fakhrai, T. Fransson, and S. Jaras, Catal. Today 100 (2005) 479.

[9] K. Persson, A. Ersson, K. Jansson, N. Iverlund, and S. Jaras, J. Catal. 231 (2005) 139.

[10] K. Persson, K. Jansson, and S. Jaras, J. Catal. 254 (2007) 401.

[11] G. Lapisardi, P. Gelin, A. Kaddouri, E. Garbowski, and S. Da Costa, Top. Catal. 42-43 (2007) 461.

[12] B. Lim, M. Jiang, P. H. C. Camargo, E. C. Cho, J. Tao, X. Lu, Y. Zhu, and Y. Xia, Science 324 (2009) 1302.

[13] T. Kondo, T. Sasaki, and S. Yamamoto, J. Chem. Phys. 118 (2003) 760.

[14] J. Han, D. Zemlyanov, and F. H. Riberio, Catal. Today 117 (2006) 506.

[15] Se. H. Oh, P. J. Mitchell, and R. M. Siewert, J. Catal. 132 (1991) 287.

[16] R. F. Hicks, M. L. Young, R. G. Li, and H. Qi, J. Catal. 122 (1990) 280.

[17] R. F. Hicks, M. L. Young, R. G. Li, and H. Qi, J. Catal. 122 (1990) 295.

[18] P. Carlsson, E. Fridell, and M. Sloglundh, Catal. Lett. 115 (2007) 1.

[19] R. Burch, P. K. Loader, and F. J. Urbano, Catal. Today 27 (1996) 243.

[20] H. Gabasch, K. Hayek, B. Klötzer, W. Unterberger, E. Kleimenov, D. Teschner, S. Zafeiratos, M. Hävecker, A. Knop-Gericke, R. Schlögl, B. Aszalos-Kiss, and D. Zemlyanov, J. Phys. Chem. C 111 (2007) 7957.

[21] E. Becker, P.-A. Carlsson, H. Grönbeck, and M. Skoglundh, J. Catal. 252 (2007) 11.

[22] V. P. Zhdanov, P. A. Carlsson, and B. Kasemo, J. Chem. Phys. 126 (2007) 234705.

[23] O. Muller and R. Roy, J. Less-Common Metals 16 (1968) 129.

[24] N. Seriani, Z. Jin, W. Pompe, and L. Colombi Ciacchi, Phys. Rev. B 76 (2007) 155421.

[25] T. Jacob, J. Electroanal. Chem. 607 (2007) 158.

[26] S. P. Devarajan , J. A. Hinojosa, Jr., and J. F. Weaver , Surf. Sci. 602 (2008) 3116.

[27] N. Seriani, W. Pompe, and L. Colombi Ciacchi, J. Phys. Chem. B 110 (2006) 14860.

[28] N. Seriani and F. Mittendorfer, J. Phys.: Condens. Matter 20 (2008) 184023.

[29] P. Nolte, A. Stierle, O. Balmes, V. Srot, P. A. van Aken, L. P. H. Jeurgens, and H. Dosch, Catal. Today, in press.

[30] J. Klikovits, E. Napetschnig, M. Schmid, N. Seriani, O. Dubay, G. Kresse, and P. Varga, Phys. Rev. B 76 (2007) 045405.

[31] H. H. Kan, R. Bradely Shumbera, J. F. Weaver, Surf. Sci. 602 (2008) 1337.

[32] J. A. Hinojosa, Jr., Howood H. Kan, and J. F. Weaver, J. Phys. Chem. C 112 (2008) 8324.

[33] P. Kostelník, N. Seriani, G. Kresse, A. Mikkelsen, E. Lundgren, V. Blum, T. Šikola, P. Varga, and M. Schmid, Surf. Sci. 601 (2007) 1574.

[34] R. Westerström, C. J. Weststrate, A. Resta, A. Mikkelsen, J. Schnadt, J. N. Andersen, E. Lundgren, M. Schmid, N. Seriani, J. Harl, F. Mittendorfer, and G. Kresse, Surf. Sci. 602 (2008) 2440.

[35] A. Dianat, N. Seriani, M. Bobeth, W. Pompe, and L. Colombi Ciacchi, J. Phys. Chem. C 112 (2008) 13623.

[36] G. Kresse and J. Hafner, Phys. Rev. B 47 (1993) 558; ibid. 49 (1994) 14251.

[37] G. Kresse and J. Furthmüller, J. Comput. Mater. Sci. 6 (1996) 15.

[38] G. Kresse and J. Furthmüller, Phys. Rev. B 54 (1996) 11169.

[39] J. P. Perdew, K. Burke, and M. Ernzerhof, Phys. Rev. Lett. 77 (1996) 3865.

[40] P. Blöchl, Phys. Rev. B 50 (1994) 17953.

[41] G. Kresse and D. Joubert, Phys. Rev. B 59 (1999) 1758.

[42] H. J. Monkhorst and J. D. Pack, Phys. Rev. B 13 (1976) 5188.

[43] A. Dianat, J. Zimmermann, N. Seriani, M. Bobeth, W. Pompe, and L. Colombi Ciacchi, Surf. Sci. 602 (2008) 876.

[44] G. Ketteler, D. F. Ogletree, H. Bluhm, H. Liu, E. L. D. Hebenstreit, and M. Salmeron, J. Am. Chem. Soc. 127 (2005) 18269.

[45] M. Todorova, E. Lundgren, V. Blum, A. Mikkelsen, S. Gray, J. Gusafon, M. Borg, J. Rogal, K. Reuter, J. N. Andersen, and M. Scheffler, Surf. Sci. 541 (2003) 101.

[46] D. Zemlyanov, B. Aszalos-Kiss, E. Kleimenov, D. Teschner, S. Zafeiratos, M. Hävecher, A. Knop-Gericke, R. Schlögl, H. Gabasch, W. Unterberger, K. Hayek, and B. Klötzer, Surf. Sci. 600 (2006) 983.

[47] H. Gabasch, W. Unterberger, K. Hayek, B. Klötzer, E. Kleimenov, M. Hävecher, D. Teschner, S. Zafeiratos, M Hävecher, A. Knop-Gericke, R. Schlögl, J. Han, F. H. Riberio, B. Aszalos-Kiss, T. Curtin, and D. Zemlyanov, Surf. Sci. 600 (2006) 2980.

[48] K. Reuter and M. Scheffler, Appl. Phys. A 78 (2004) 793.

[49] C. Stampfl, A. Soon, S. Piccinin, H. Shi, and H. Zhang, J. Phys.: Condens. Matter 20 (2008) 184021.

[50] J. Rogal, K. Reuter, and M. Scheffler, Phys. Rev. B 69 (2004) 075421.

[51] C. Ellinger, A. Stierle, I. K. Robinson, A. Nefedov, and H. Dosch, J. Phys.: Condens. Matter 20 (2008) 184013.

[52] J. F. Weaver, H. H. Kan, and R. B. Bradley, J. Phys.: Condens. Matter 20 (2008) 184015.

[53] M. Todorova, K. Reuter, and M. Scheffler, Phys. Rev. B 71 (2005) 195403.

[54] R. B. Getman and W. F. Scheider, J. Phys. Chem. C 112 (2008) 9559.

[55] R. F. W. Bader, Accounts Chem. Res. 18 (1985) 9.

[56] G. Henkelman, A. Arnaldsoon, and H. Jønsoon, Comput. Mater. Sci. 36 (2006) 354.

[57] G. Novell-Leruth A. Valcarcel, J. Perez-Ramirez, and J. M. Ricart, J. Phys. Chem. C 111 (2007) 860.

[58] C.-T. Au, C.-F. Ng, and M.-S. Liao, J. Catal. 185 (1999) 12.

[59] J. F. Paul and P. Sautet, J. Phys. Chem. B 102 (1998) 1578.

[60] C. J. Zhang and P. Hu, J. Chem. Phys. 116 (2002) 322.

[61] M. Blanco-Rey and S. J. Jenkins, J. Chem. Phys. 130 (2009) 014705.

[62] F. Gao, Y. Wang, Y. Cai, and D. W. Goodman, J. Phys. Chem. C 113 (2009) 174.

[63] G. Fratesi, P.Gava, and S. de Gironcoli, J. Phys. Chem. C 111 (2007) 17015.

[64] A. Holmen, Catal. Today 142 (2009) 2.

Tables

Table 1: Calculated average oxygen binding energies (in eV) in the case of only on-surface adsorption (on) and for simultaneous on-surface and sub-surface adsorption (on+sub) on Pd(111), Pt(111), and Pd/Pt/Pd(111) at different O coverages. In the on+sub case, the amount of sub-surface oxygen is always 0.25 ML and the remaining oxygen is on the surface, i.e. for 0.25 ML total coverage there is no oxygen on the surface in the on+sub case.

Total O coverage	Pd(111)		Pt(111)		Pd/Pt/Pd(111)	
in ML	on	on+sub	on	on+sub	on	on+sub
0.25	-1.34	0.36	-1.22	0.68	-1.39	0.64
0.50	-1.03	-0.93	-0.92	-0.52	-1.06	-0.85
0.75	-0.61	-0.72	-0.55	-0.47	-0.69	-0.68
1.00	-0.22	-0.42	-0.17	-0.27	-0.25	-0.41

Table 2: Calculated adsorption energies (in eV) for the dissociative adsorption of methane on clean (111) and (100) surfaces of Pd, Pt, and Pd/Pt/Pd, and on surfaces covered with 1 ML oxygen *on* the surface, as well as with 0.75 ML on the surface and 0.25 ML in sub-surface positions. For clean surfaces, the values in squared brackets (in italics) correspond to adsorption energies within LDA. In the calculations, the initial positions of CH_3 and H have been chosen on high-symmetry sites of the (111) metal surface: CH_3 on top of metal atom (-top) and H on fcc hollow site on top of oxygen (-fcc) in case of the clean surfaces. For the systems with sub-surface oxygen, two fcc sites have been considered, CH_3 on fcc hollow site on oxygen atom (-fcc) and CH_3 on oxygen vacancy (-fcc*). The values in parentheses are the adsorption energies of methanol formation on the surfaces, irrespective of the reaction path. (These value are not related to the initial CH_3 and H positions in the table, and are arbitrarily reported besides the corresponding highest energy values obtained for the other initial configurations).

Clean surfaces					
Pd(111)	Pt(111)	Pd/Pt/Pd(111)	Pd(100)	Pt(100)	Pd/Pt/Pd(100)
0.19 *[-0.43]*	-0.08 *[-0.66]*	0.22 *[-0.45]*	0.29	-0.31	0.35

1 ML oxygen on (111) surfaces			
	CH_3-top & H-fcc	CH_3-fcc & H-fcc	CH_3-hcp & H-fcc
Pd(111)	-2.42	-1.65	-1.39
Pt(111)	-2.13 (-2.27)	-1.62	-1.99
Pd/Pt/Pd(111)	-2.47	-1.74	-1.70

0.75 ML oxygen on-surface/0.25 ML oxygen sub-surface			
	CH_3-top & H-fcc	CH_3-fcc & H-fcc	CH_3-fcc* & H-fcc
Pd(111)	-0.80	-1.59 (-1.87)	-0.75
Pt(111)	-1.39	-1.40 (-1.78)	-1.23
Pd/Pt/Pd(111)	-0.95	-1.28 (-1.88)	-0.61

Table 3: Calculated methane adsorption energies (in eV) on the (101) and (100) surfaces of the PdO bulk oxide phase with one mixed oxide surface layer $Pd_{1-x}Pt_xO$.

Structure	x=0	x=0.25	x=0.5	x=0.75	x=1
PdO(101)	-0.37	-0.63	-0.82	-0.61	-0.45
PdO(100)	-1.00	-0.94	-0.57	-0.51	-0.18

Figures

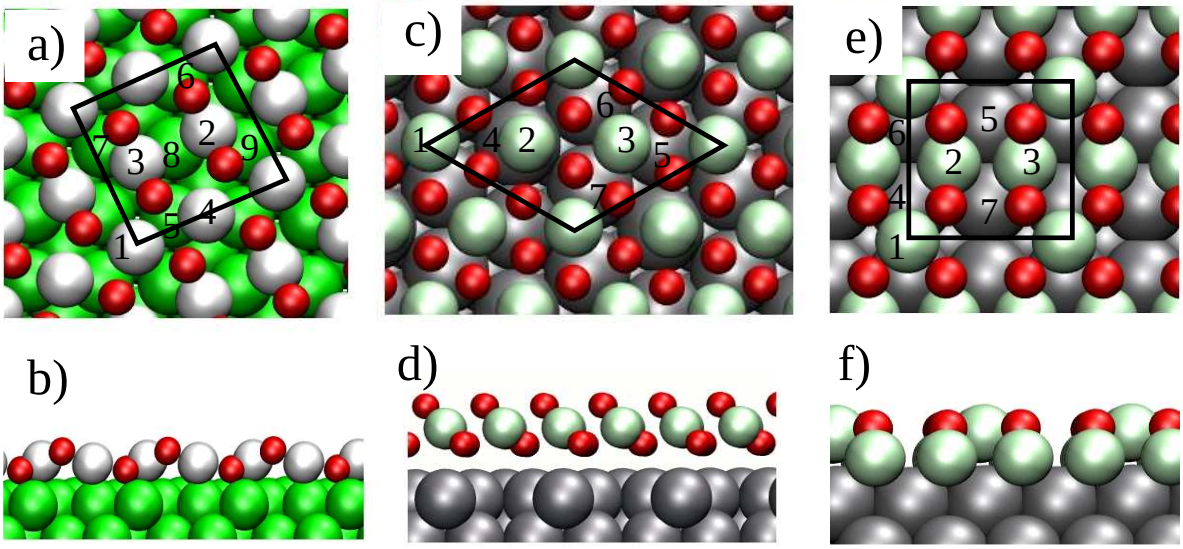

Figure 1: Top- and side-views of optimized atomic structures of different oxide layers: (a,b) PdO(101) on Pd(100), (c,d) α-PtO_2(0001) on Pt(111), and (e,f) Pt_3O_4(100) on Pt(100) (O - red small spheres, metal - large spheres). In the case of mixed oxide and surface metal layers, Pd atoms are replaced by Pt (and vice versa) as described in the text.

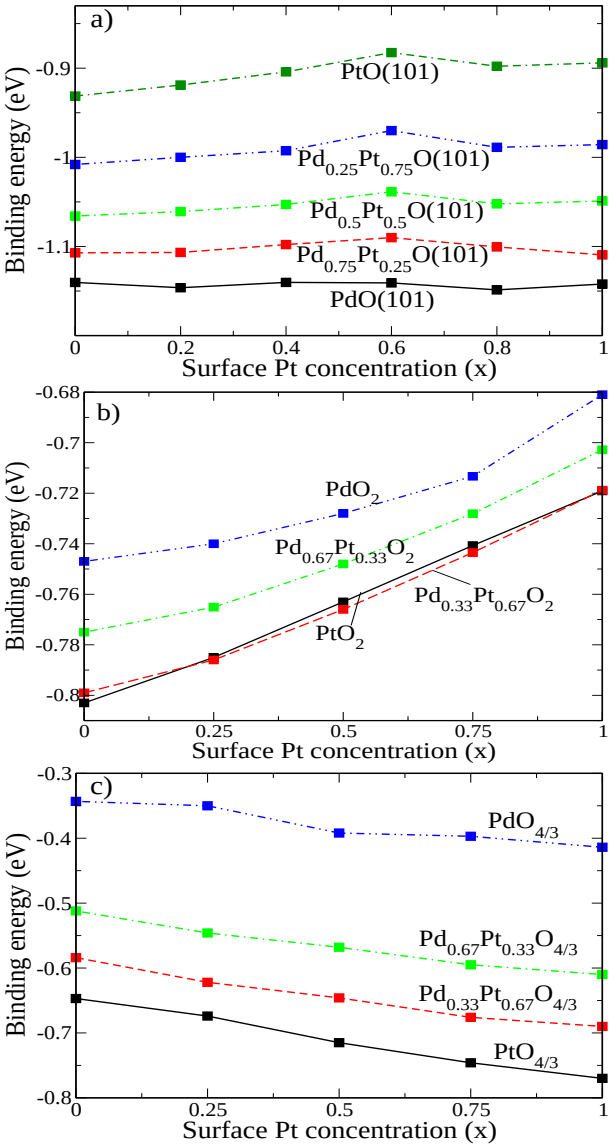

Figure 2: Calculated average binding energies of oxygen for different oxide layer structures as a function of the Pt concentration x of the outermost substrate layer. The different curves correspond to different compositions of the oxide layer, as indicated by the labels. (a) $Pd_{1-y}Pt_yO(101)$ on $Pd_{1-x}Pt_x/Pd(100)$, (b) α-$Pd_{1-y}Pt_yO_2(0001)$ on $Pd_{1-x}Pt_x/Pt(111)$, and (c) $Pd_{1-y}Pt_yO_{4/3}(100)$ on $Pd_{1-x}Pt_x/Pt(100)$.

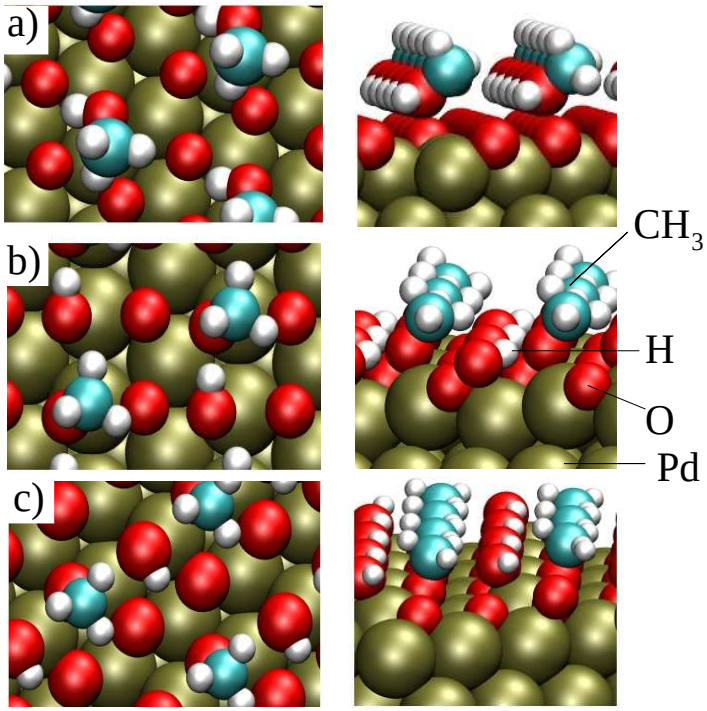

Figure 3: Optimized atomic structures of adsorbed CH_3 and H on a Pd(111) metal surface covered with 1 ML oxygen. In the calculations the initial lateral positions of CH_3 and H have been chosen as follows: a) CH_3 on top of a metal atom and H on top of oxygen, b) CH_3 and H on top of oxygen atoms, and c) CH_3 on hcp hollow site and H on top of oxygen. The largest adsorption energy is obtained for a). Distances between adsorbed atoms and nearest neighbor substrate atoms in Å: a) $d_{C-Pd} = 4.00$, $d_{C-O} = 1.43$, $d_{H-O} = 0.98$; b) $d_{C-Pd} = 3.04$, $d_{C-O} = 1.41$, $d_{H-O} = 1.00$; c) $d_{C-Pd} = 3.05$, $d_{C-O} = 1.40$, $d_{H-O} = 0.98$.

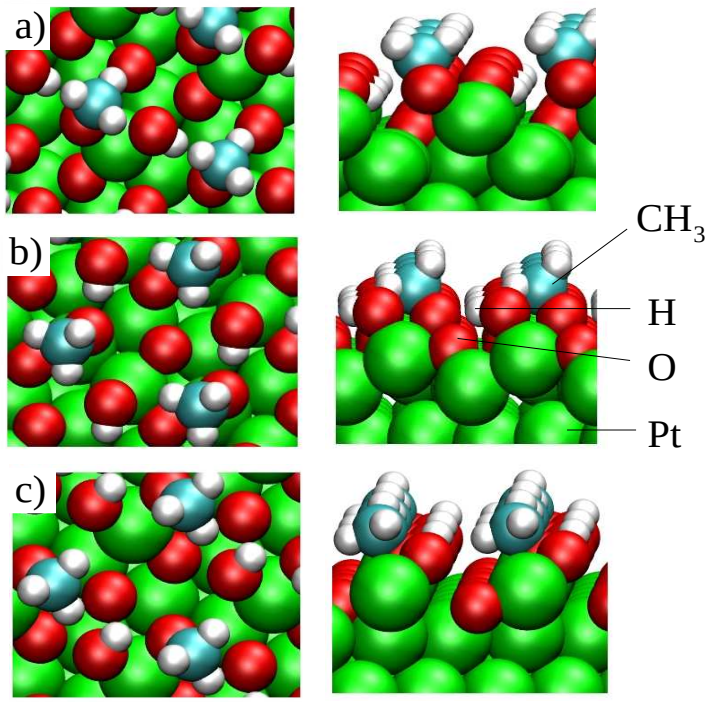

Figure 4: Optimized atomic structures of adsorbed CH_3 and H on a Pt(111) metal surface covered with 1 ML oxygen. In the calculations the initial lateral positions of CH_3 and H have been chosen as follows: a) CH_3 on top of a metal atom and H on top of oxygen, b) CH_3 and H on top of oxygen atoms, and c) CH_3 on hcp hollow site and H on top of oxygen. The largest adsorption energy is obtained for a). Distances between adsorbed atoms and nearest neighbor substrate atoms in Å: a) $d_{C-Pd} = 2.97$, $d_{C-O} = 1.42$, $d_{H-O} = 0.99$; b) $d_{C-Pd} = 3.03$, $d_{C-O} = 1.41$, $d_{H-O} = 1.00$; c) $d_{C-Pd} = 2.92$, $d_{C-O} = 1.41$, $d_{H-O} = 1.00$.

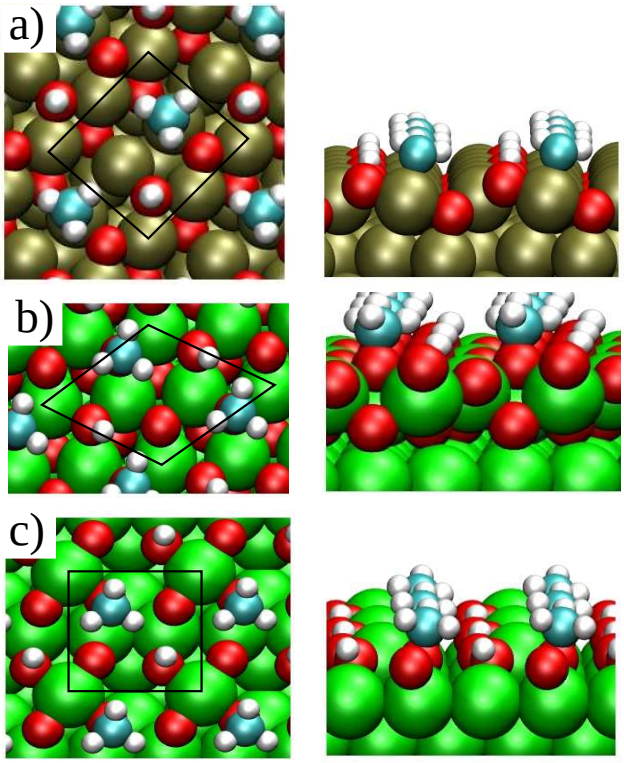

Figure 5: Optimized atomic structures of adsorbed CH_3 and H on thin oxide layers of pure a) PdO(101)/Pd(100), b) α-PtO_2(0001)/Pt(111), and c) Pt_3O_4(100)/Pt(100). The shown atomic configurations correspond to the highest adsorption energy for each oxide layer. Distances between adsorbed atoms and nearest neighbor substrate atoms in Å: a) $d_{C-Pd} = 2.05$, $d_{C-O} = 2.77$, $d_{H-O} = 0.98$; b) $d_{C-Pd} = 3.15$, $d_{C-O} = 1.43$, $d_{H-O} = 0.98$; c) $d_{C-Pd} = 2.85$, $d_{H-O} = 0.98$, $d_{C-O} = 1.44$.

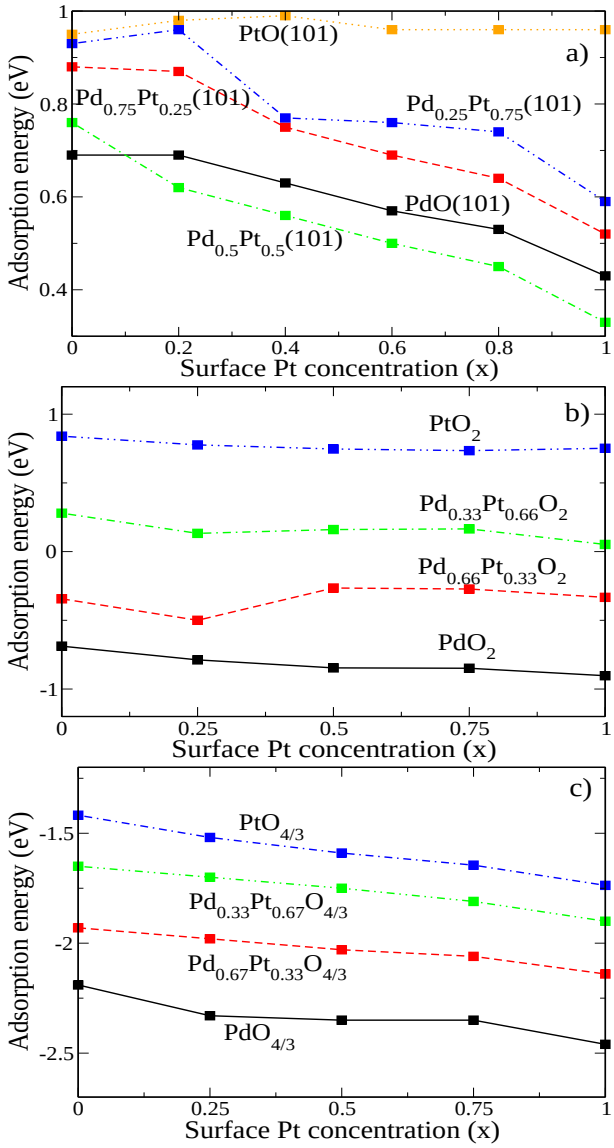

Figure 6: Calculated methane adsorption energies on thin Pd-Pt oxide layers as a function of the Pt concentration x in the metal surface layer with the Pt concentration y in the oxide as a parameter: (a) $Pd_{1-y}Pt_yO(101)/Pd_{1-x}Pt_x/Pd(100)$, (b) α-$Pd_{1-y}Pt_yO_2/Pd_{1-x}Pt_x/Pt(111)$, and (c) $Pd_{1-y}Pt_yO_{4/3}/Pd_{1-x}Pt_x/Pt(100)$.

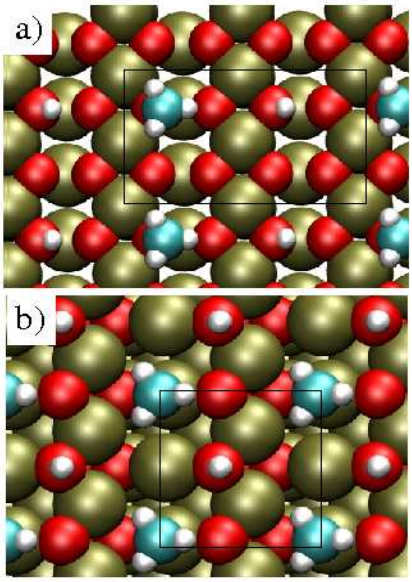

Figure 7: Optimized atomic structures of adsorbed CH_3 and H on the a) (100) and b) (101) surface of the bulk oxide phase PdO. Distances between adsorbed atoms and nearest neighbor substrate atoms in Å: a) $d_{C-Pd} = 2.96$, $d_{C-O} = 1.47$, $d_{H-O} = 0.99$; b) $d_{C-Pd} = 2.04$, $d_{C-O} = 2.81$, $d_{H-O} = 0.98$.